Reaction Chemistry & Engineering

ROYAL SOCIETY OF CHEMISTRY

PAPER

View Article Online
View Journal | View Issue

Cite this: *React. Chem. Eng.*, 2024, **9**, 1364

A machine learning based approach to reaction rate estimation†

Matthew S. Johnson and William H. Green *

Chemical kinetic models are vital to accurately predicting phenomena in a wide variety of fields from combustion to atmospheric chemistry to electrochemistry. However, building an accurate chemical kinetic model requires the efficient and accurate estimation of many reaction rate coefficients for many reaction classes with highly variable amounts of available training data. Current techniques for fast automatic rate estimation tend to be poorly optimized and tedious to maintain and extend. We have developed a machine learning algorithm for automatically training subgraph isomorphic decision trees (SIDT) to predict rate coefficients for arbitrary reaction types. This method is fully automatic, scalable to virtually any dataset size, human readable, can incorporate qualitative chemical knowledge from experts and provides detailed uncertainty information for estimates. The accuracy of the algorithm is tested against the state of the art rate rules scheme in the RMG-database for five selected reaction families. The SIDT method is shown to significantly improve estimation accuracy across all reaction families and considered statistics. The estimator uncertainty estimates are validated against actual errors.

Received 17th December 2023,
Accepted 13th February 2024

DOI: 10.1039/d3re00684k

rsc.li/reaction-engineering

1 Introduction

Automatic, rapid and accurate estimation of reaction rates is critical in the development of large chemical kinetic models. Kinetic models can contain tens of thousands of kinetic parameters[1] and the construction processes require estimation of many more to decide which reactions are fast enough to be important. Furthermore, chemical kinetic models are only increasing in size requiring estimation of more and more rate coefficients. Rate based automatic mechanism generation relies even more on accurate estimates as the quality of these estimates affects the species and reactions included.[2–5]

While quantum chemistry calculations can be used to estimate reaction rates to high accuracy, they are not fast and not yet fully automatic. Although computers continue to become faster, high accuracy quantum chemistry calculations can take days to weeks to run. Furthermore, there are often difficulties in finding the transition state of a particular reaction, requiring human intervention, making the process even slower.

Much progress is being made on automatic high accuracy rate calculations based on transition state finding algorithms such as Kinbot, nudged elastic band, HFSP, AFIR, and string methods[6–12] and workflow codes such as ARC, Pynta, KinBot, and AutoMech.[6,9,13,14] However, for the moment these methods are computationally expensive and not entirely robust, with only limited benchmarking.[15,16] But even if these methods were robust, it would probably be impractical to use them to compute all the rate coefficients of interest (though perhaps this assessment could change after exascale computers become widely available).

Our group has used these automated methods to construct a large dataset of DFT transition state (TS) geometries[17] and a corresponding dataset of CCSD(T) barrier heights.[18] These datasets have been used to train machine learning models that provide useful initial guesses at TS geometries[19] and estimates of barriers for a certain class of reactions of small closed-shell molecules.[20] The neural-net modeling methods we developed for these tasks[19,21,22] have some promise, but are still far from perfect; among other problems they require huge training sets of accurate transition states or barriers, and at present the uncertainties in each prediction is unknown. This latter problem is important because even if the average prediction error is acceptably small, a significant percentage of the rate predictions can be completely wrong, with no warning to the user.

Department of Chemical Engineering, Massachusetts Institute of Technology, Cambridge, MA 02139, USA. E-mail: whgreen@mit.edu

† Electronic supplementary information (ESI) available: The software and datasets used here are available on GitHub in the RMG-Py and RMG-database repositories. A Jupyter notebook is available in the RMG-database repository for generating and fitting kinetics trees as done in this work. The specific code and database states used in this work are available on the sidt_paper branches of these repositories. The supporting information contains error histograms for radical recombination, disproportionation and keto-enol reaction families. See DOI: https://doi.org/10.1039/d3re00684k

Fast accurate kinetics estimation for reaction mechanisms is a difficult problem. Fundamentally, the 2-D structures of the reactants (typical of reaction mechanisms), the atom mapping, the type of reaction and the thermodynamic information for the reactant and product must be mapped to a temperature dependent reaction rate. The problem is very different from thermodynamic property prediction.

Thermodynamic properties typically have very linear relationships with their molecular structures due to the fact that the thermodynamic properties (H_{f298}, S_{f298}, $C_p(T)$) of a molecule are approximately equal to the sum of the thermodynamic contributions of its individual substructures.[23] One can try a similar approach to estimate the thermochemistry of transition states,[24] but it requires a much larger set of substructures. Unlike thermochemical properties, reactions both have many different types and are much more difficult to calculate. This means that it requires larger datasets to train rate estimation algorithms and the available datasets are much sparser. These properties necessitate particular care when designing algorithms for estimating the rates of chemical reactions.

The most traditional approach to quickly estimating reaction rates in mechanism construction is rate rules (RR).[2,4,25] Abstractly a rate rule maps all reactions with specific substructures around the atoms participating in the reaction to a specified reaction rate. These substructures for hydrogen abstraction might look something like R–CH_2–R*(·) H–CH_3 + H*–CH_2–R. A reaction is estimated using the rate rule corresponding to the most specific substructures it matches that a rate rule is known for. These rate rules and associated substructures are usually written by hand. The RR system used by the reaction mechanism generator (RMG) software uses an improved version of this that allows use of a set of training reactions.[2,4] In this formulation for a given tree structure (see Fig. 1) training reactions descend down the tree (following the substructures they match) and become additional rate rules at the most specific node they match. This allows rules to be generated from training data given a fixed tree structure. The RR approach suffers from two primary disadvantages: (i) the rules must be constructed manually, taking substantial human time and effort to update and improve and (ii) the accuracy of RR depends on the assumed tree structure.

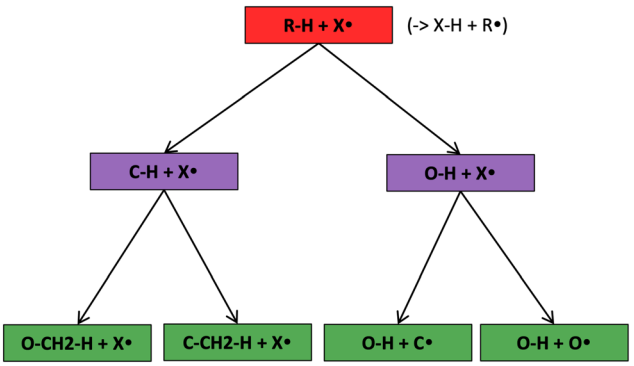

Fig. 1 Example of a subgraph isomorphic reaction template decision tree.

Other approaches have used reaction group additivity.[24,26–29] Reaction group additivity works much like thermodynamic group additivity except that instead of adding linear components from specific atoms to estimate thermodynamic parameters linear components are added from specific substructures of the reaction mapping to estimate kinetic parameters. The substructures follow a set of manually written trees for each reaction type and then the contribution to each kinetic parameter at each substructure is fit linearly to a set of reaction rates. Most often the kinetic parameters used are the logarithm of the components of the modified Arrhenius form $\log(A) + n\log(T) - \frac{E_a}{RT}$, where A, n, E_a are the Arrhenius parameters, R is the gas constant and T is the temperature. The performance of reaction group additivity is in general mixed. When applied to limited regions of chemical space that are well covered with data, good performance can be achieved.[24,26,28] However, so far when applied to large chemical spaces where the data is more sparse, such as the training set for RMG's estimators, performance has been poor compared to RR.[29] Additionally, reaction group additivity much like RR must be manually formulated and the accuracy is limited by that formulation.

Most recently neural nets, decision trees and genetic algorithms have been applied to predicting kinetic parameters.[17,20,30,31] However, these efforts have so far focused on either activation energies or on rates at a single temperature. So far these models are not suitable for large scale temperature dependent rate estimation. Furthermore, these methods tend to require large amounts of data, are rarely human readable or adjustable, and often lack uncertainty estimates.

The uncertainties in rate coefficients have been studied extensively. In the early days of kinetics individual uncertainty factors were estimated based mostly on reviews of available experimental data.[32] As this area developed, the importance of properly accounting for correlations in rate coefficients and experimental data was established.[33] Later work developed techniques such as spectral methods for quantifying these correlated uncertainties properly.[34–36] Detailed work has also been done on quantifying the uncertainty in rate coefficients based on quantum chemistry calculations.[37–39] The temperature dependence and correct form of these uncertainties has also been studied in detail.[40]

Ideally a kinetics estimator would be nonlinear, scalable to different dataset sizes (as the amount of available data varies dramatically for different types of reactions), fast, accurate, capable of uncertainty estimation, automatically trainable, human readable, and able to incorporate qualitative chemical knowledge. However, each of the prior methods discussed here lacks at least one of these characteristics. For this reason we present a new approach, the subgraph isomorphic decision tree (SIDT), a rate estimator with all of the above desirable properties.

2 Theory and implementation

In the following, we will discuss in detail our rationale for approaching kinetics estimation using decision trees. We will then introduce the structure of SIDT's and discuss the algorithm we use for training them. Furthermore, we will describe how to estimate kinetics from an SIDT and how to predict associated uncertainties in that estimate. We will also discuss further important details such as regularization, scaling and performance optimization.

2.1 Structure

Modern estimators that can be retrained automatically on new datasets are generally the realm of machine learning. While graph convolutional neural networks are quite popular for predicting molecular properties there are a number of downsides for this particular application. Neural networks require large training datasets to get accurate results. Little research has been done particularly in kinetics estimation to work out how much data is required. It seems unlikely that datasets smaller than 300 reactions could be used to train a viable neural network. Successful published studies have used datasets containing more than 10 000 reactions.[17,20,30] Most reaction families in the RMG database are estimated from fewer than 20 reactions, and the largest families only contain around 3000 reactions.[3,4] For this reason a decision tree estimator was investigated. Decision trees can work with almost any training set size and have the additional advantage of generally being much easier for humans to interpret than neural networks.

Decision trees are classifiers that start with an item at a single root node with no parents. At each node the item is checked against each descendant "child" node and moves to the first child node that it matches and so on until it reaches a node where it doesn't match any children. That final node becomes its classification.[41] In traditional decision trees the item might be a fingerprint and "matching" might be determined by checking if a specific component of the fingerprint is zero or is greater than 1. In our context the items are reactions, essentially, molecular graphs of reactant(s) and product(s) with atom mapping (*e.g.* condensed graph of reaction (CGR) format)[22,42] and matching can be done by subgraph isomorphism checks. See Fig. 1 for one example of a subgraph isomorphic reaction template decision tree.

2.2 Training strategy

Such decision trees have been used within RMG for many years.[43] However they are tedious to construct, update and maintain and their accuracy is dependent on the knowledge of the kineticists that build and maintain them. In order to automatically construct an optimal tree one could imagine searching the space of all possible decision trees. However, typically it is infeasible to do this on a given dataset due to the high dimensionality of the problem.[41] It is standard instead to iterate starting from a single root node adding the new node that best optimizes the tree each iteration. The tree generation process typically ends when some termination criterion related to the number of tree nodes or tree depth is satisfied.

This greedy optimization approach in our case starts to look like the diagram in Fig. 2. One starts with an initial tree (possibly only containing a single node) and a set of training reactions classified to the bottom nodes of the initial tree. We

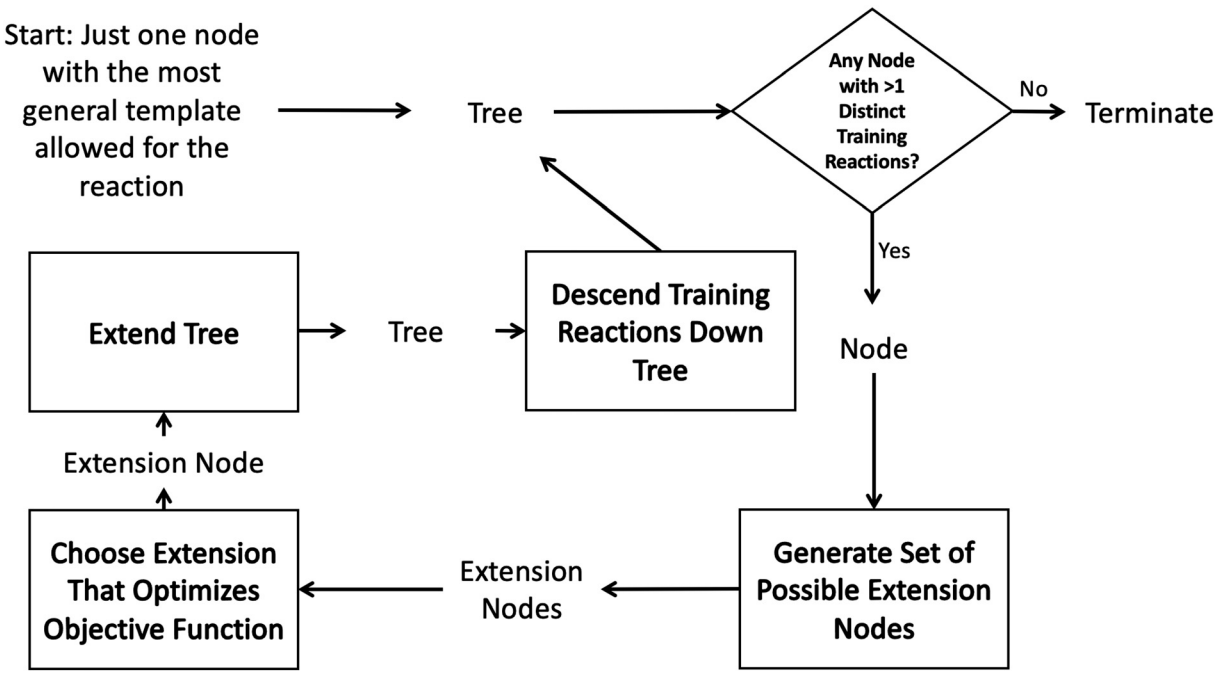

Fig. 2 Decision tree estimator generation algorithm.

then choose any node in the tree with more than one training reaction and attempt to add new nodes that best divide those reactions into groups with similar rate estimates. This involves generating a set of possible new nodes and selecting the best extension node. After the new node is selected it is added to the tree and the training reactions are descended down to the most specific node they match. Then the iterative procedure is continued with a new node.

2.3 Generating extension nodes

Each iteration the algorithm must generate a set of group structures subgraph-isomorphic to the structure at the chosen node. An example of extension generation is displayed in Fig. 3. The root (first) structure in the tree is user specified. Consider a simple structure: R–C*$\overset{?}{-}$R where * denotes an atom that participates in the reaction in a way that makes it unique, ? denotes a bond that has an unknown order and *R* denotes an unspecified atom. Most real reaction templates are more complex, but this example structure is convenient for illustrating important concepts. Structures that would match this include the following: C^*H_3–CH_3, CH_3–C^*H_2–NH_2, NH_2–C*H═CH_2, CH_3–C*H(–CH_3)–OH, and C^*H_2–CH_3.

In this context it is relatively easy to start listing off ways to make atoms and bonds in R–C*$\overset{?}{-}$R more specific. We call these specification extensions. We allow the definition of the element of an atom or the order of a bond. We also need some way to specify the presence of a radical which we add by allowing extensions to specify the number of unpaired electrons on an atom. One could also imagine situations where the charge on an atom or the number of paired electrons is important. We allow one last specification extension that specifies if an atom is in a ring or not; the significance of this will be discussed later in this paper.

To ensure we can divide arbitrary sets of reactions we need to be able to create new bonds and atoms in the structures. For this reason we define (1) an internal bond creation extension that forms bonds of undefined order between atoms present in the structure and (2) an external bond creation extension that forms a bond of undefined order between an atom in the structure and a new R!H (any atom but H).

There are a couple of nuances here. The first is that while one could define an extension that adds an unattached unspecified atom to the structure it is unlikely to provide more useful splitting than an attached unspecified atom. By extending with R!H rather than R we have made it impossible to add hydrogens to an atom in the structure. However, this only means that the way we divide reactions that have hydrogens in those locations from those that do not is by defining bonds to R!H that will only match those without hydrogens. In particular this also significantly reduces the number of extensions generated; which will be quite important later.

So far we have described individual one-step extensions we can apply to a structure, but we have not determined how

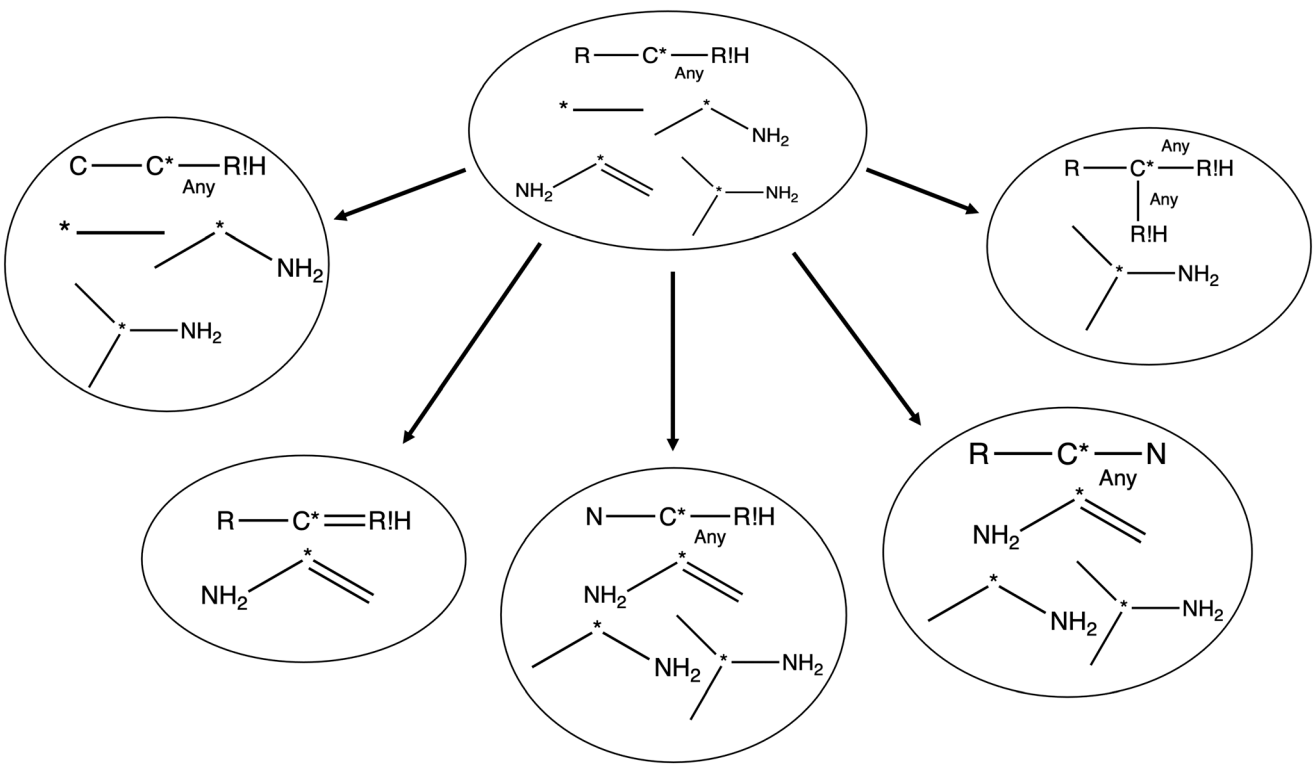

Fig. 3 Extension generation example. Includes only nodes that split the reaction set.

we should concatenate them to generate the considered set of extensions. Naively one might consider applying extensions in N-steps where the set of one-step extensions is generated off the original structure, and then extensions off those structures and so on eventually combining them all into one set of possible extensions. However, even beyond making the number of structures combinatorically large this approach is insufficient to divide all sets of reactions.

There are a few important things to understand in these cases. First, when a selected extension is compared with the set of reactions there are three possible results: it matches none of the reactions, it matches some of the reactions or it matches all of the reactions. Second, specification extensions as defined in this study are only useful for purposes of extension selection if they match some of the reactions. Third, bond creation extensions are important when they match some or all of the reactions. Consider our structure from before R–C*$^{\underline{?}}$R and suppose our reactions can be represented: CH_3–C*H_2–CH_2–CH_2–CH_3, CH_3–C*H_2–CH_2–OH and CH_3–C*H_2–CH_2–CH═O. Using one-step extensions this set of reactions cannot be divided because every one-step extension either matches all or none of the reactions. If we were to only have CH_3–C*H_2–CH_2–CH_2–CH_3 and CH_3–C*H_2–CH_2–CH═O in fact two-step extensions would be insufficient as well. This situation is common since training reaction data are sparse. It is particularly important in reactions that involve rings.

In order to get around these issues and run efficiently we start by generating one-step extensions from the original structure. If a bond creation extension matches all of the reactions the identified tags from that iteration are applied to it and then it is treated like the original structure and first step extensions are generated for it and so on. Each specification extension that matches none of the reactions is tagged for future reference and not generated again. For example if H–C*$^{\underline{?}}$R is found to not match any structures under R–C*$^{\underline{?}}$R we don't generate the atomic extensions of that particular R again when we examine R–C*$^{\underline{?}}$R–$^{?}$R!H. After this recursive procedure is run, all generated extensions that match some, but not all, of the reactions are combined to form the set of considered extensions.

Note that when we recurse on the bond creation extensions we do recheck specification extensions that matched all reactions before, even though it might seem like this would be true for all descendent structures. This is because a specification extension that matches all reactions can in some cases stop matching reactions as the structure is extended. Consider the node C*–R!H with reaction templates HO–H_2C*–NH–CH_3 and H_2C*(–NH_2)–O–CH_3. Naturally the algorithm will extend C*–R!H to C*(–R!H)–R!H–R!H. However, by the time C*(–R!H)–R!H–R!H is generated the algorithm will have tagged atom extensions on the R!H atoms bonded to C* and found that both N and O match all of the reactions. If each generalization between the group and its reactions was fixed (only N or only O in the case above) it would be safe to assume a specification extension that matched all reactions would match all reactions for all subgraph isomorphic groups that matched a reaction in the set because it would be the same. However now that the third R!H is added specifying the atom type of one of the R!H atoms bonded to C* is the only way to divide the two reactions. If we were to not recheck specifying atom types for those atoms it would be impossible to divide the reaction set.

2.4 Choosing the best extension

The best extension to add to a rate tree should be the one that improves estimation the most after adding it. In an ideal situation one would fit all of the data on each side of the split to a model of choice for nodes in the tree and then run leave-one-out cross validation at a variety of temperatures to determine the differences in errors. However, our model parameters (which will be discussed later) are not analytic functions of the data, so such an analysis would be very computationally expensive.

Using a variety of temperatures is also problematic. Quantum chemical rate calculations are much more accurate at higher temperatures than lower temperatures and experimental rates are often only accurate in a specific temperature range. As a result the RMG database we draw our training sets from contains many rates that aren't accurate at low or very high temperatures, however accuracy for most rates is good in the vicinity of 1000 K.

For these reasons in this work we choose extensions based on accuracy improvement at 1000 K assuming errors in the rate coefficient are lognormally distributed. We choose the extension that minimizes

$$\Pi = N_1\sigma_1 + N_2\sigma_2 \quad (1)$$

where N_i is the number of reactions in partition i and σ_i is the standard deviation in $\log(k(1000\ \mathrm{K}))$ within partition i. We therefore choose the extension that clusters reactions with similar rates into the same partitions. It should be relatively easy to extend this to more complex schemes in the future. We can continue to extend the tree in this manner until each leaf node contains a single training reaction.

2.5 Extending the tree: complementary nodes

Once an extension is selected it is added to the decision tree under its parent node. If the extension does not create any bonds it is usually possible to define a complementary node that matches any reaction that matches the parent, but does not match the new node. For example if an R is defined as being a H the complement would be the same structure with R as R!H. If such a complementary node can be defined it is also added under the parent. Then reactions are descended from the parent to any of the new nodes they match.

Adding complementary nodes improves readability. Suppose we have a parent node R–C*–$^{?}$R!H, we select a first child node H–C*–$^{?}$R!H and we do not define a complementary node. Since we still have reactions at the parent node we need to generate a second child node. For example we might generate R–C*–$^{?}$R!H–$^{?}$R!H a structure that isn't mutually exclusive with the other child. However, because the first child comes first in the tree no structure that matches it will be matched to the second child. This means that the R in reactions matching the second child will never be H so the second child would be more clearly written as R!H–C*–$^{?}$R!H–$^{?}$R!H. Adding complementary nodes when possible makes the generated tree structure easier for a human to read.

2.6 Estimating rates from the tree

Now that we have a tree we need to define precisely how we use that tree to estimate rates. We define a rule at each node. In order to do this we take all the reactions that match a given node (so the top node would have all reactions) and fit them to a Blowers–Masel interpolant.[44] This interpolant developed in Blowers and Masel 2000 correlates ΔH_r with E_a in a way that is much more accurate across the range of ΔH_r values than other more typical forms such as Evans–Polanyi.[44] The interpolant is defined by the equations

$$E_a = \begin{cases} 0 \text{ if } \Delta H_r < -4E_a^0 \\ \Delta H_r \text{ if } \Delta H_r > 4E_a^0 \\ \text{else } \dfrac{\left(w_o + \dfrac{\Delta H_r}{2}\right)\left(V_p - 2w_o + \Delta H_r\right)^2}{V_p^2 - 4w_o^2 + \Delta H_r^2} \end{cases} \quad (2)$$

$$V_p = 2w_o \frac{w_o + E_a^0}{w_o - E_a^0} \quad (3)$$

$$w_o = \frac{w_B + w_F}{2} \quad (4)$$

$$k(T) = AT^n e^{\frac{-E_a}{RT}} \quad (5)$$

where ΔH_r is the heat of reaction, w_B is the bond dissociation energy of bonds breaking and w_F is the bond dissociation energy of bonds forming, E_a^0 is referred to as the intrinsic barrier to reaction, and A and n are Arrhenius parameters.[44] This interpolant is controlled by four parameters: A, n, E_a^0 and w_o. While one can fit all four of these parameters to set of rate coefficients, the rate isn't very sensitive to w_o, which can cause problems during fitting.[44] For this reason w_o was calculated using eqn (4) with w_B and w_F estimated from tabled bond dissociation energy values for each reaction. The remaining parameters: A, n, E_a^0 were fit using weighted non-linear least squares to the rate coefficients for each training reaction in the temperature range of 300–1500 K

$$A, n, E_a^0 = \arg\min_{A,n,E_a^0} \sum_i^{N_{rxns}} \sum_j^{N_T} \left(\frac{RT_j}{\Delta E_{ij}}\right)^2 \left(\log\left(k_i(T_j)\right) - \log\left(k\left(T_j; A, n, E_a^0\right)\right)\right)^2 \quad (6)$$

where E_{ij} is the estimated error in $\log(k_i(T_j))$, N_{rxns} is the number of reactions, N_T is the number of temperatures, $k(T; A, n, E_a^0)$ is the Blowers–Masel fitting form from the above equations.

There are errors in $k_i(T_j)$ values, whatever their source, but some $k_i(T)$ values are very accurate. It is therefore important to assign different uncertainties ΔE_{ij} to different data. Considering the known inaccuracies in the experimental techniques several approaches have been employed to estimate uncertainties. One approach is for experts to consider all the (mostly experimental) data about individual reactions.[32] Another is to further constrain $k_i(T)$ using system measurements (*e.g.* flame speeds).[33–35] If the estimate is from theoretical calculations one can try to bound the errors due to each approximation, or more commonly compare the present reaction to other similar reactions, with known errors, computed using the same technique.[37,38] RMG currently has a mix of uncertainty estimates, some very accurate but many quite rough.

If $E_a^0 < 0$ the Blowers–Masel interpolant is no longer valid and we simply take averages of the parameters in our log-modified-Arrhenius expressions for each training reaction instead

$$A = \exp\left(\frac{1}{N_{rxns}} \sum_i^{N_{rxns}} \log(A_i)\right) \quad (7)$$

$$n = \frac{1}{N_{rxns}} \sum_i^{N_{rxns}} n_i \quad (8)$$

$$E_a = \frac{1}{N_{rxns}} \sum_i^{N_{rxns}} E_{a_i} \quad (9)$$

where X_i denotes the corresponding modified Arrhenius parameter of reaction i.

2.7 Estimating uncertainties from the tree

Estimating useful uncertainties for the input reactions, the interpolant, and particularly for the $k(T)$ estimate for a new reaction where no data is available, is quite challenging. Most earlier attempts[32–34,40] at estimating errors in rate estimates have been fairly heuristical, and many focused on not overestimating uncertainties for purposes of uncertainty analysis of full kinetic models.[45,46] Here we present an automated approach focused on representing the distribution of uncertainties of each $k(T)$ estimate.

We are interested in the distribution of $\Delta\log(k_i) = \log(k_{model_i}) - \log(k_{true_i})$. For an individual training reaction rate coefficient k_{rxn_i} we assume that

$$\log(k_{\mathrm{rxn}_i}) \sim N\left(\log(k_{\mathrm{true}_i}), \sigma^2_{\mathrm{rxn}_i}\right) \quad (10)$$

where N denotes the normal distribution, k_{true_i} is the true rate coefficient for reaction i and $\sigma^2_{\mathrm{rxn}_i}$ is the variance of $\log(k_{\mathrm{rxn}_i})$ based on the uncertainty in the training reaction. We assume that the Blowers–Masel estimate of a particular reaction i, k_{model_i} is distributed as

$$\log(k_{\mathrm{model}_i}) \sim N\left(\log(k_{\mathrm{best\,fit}_i}), \sigma^2_{\mathrm{model}_i}\right) \quad (11)$$

where $\sigma^2_{\mathrm{model}_i}$ is the variance associated with errors in the the Blowers–Masel parameters and $k_{\mathrm{best\ fit}_i}$ is the output the Blowers–Masel model would give without any errors in the parameters. This hypothetical errorless Blowers–Masel is what would be achieved by fitting to an arbitrarily large number of training reactions with $\sigma_{\mathrm{rxn}_i} = 0$ that match the associated node. Such an ideal model would have $\sigma_{\mathrm{model}_i}$, but still have error associated with the limitations of the Blowers-Masel fit form causing $k_{\mathrm{best\ fit}_i} \neq k_{\mathrm{true}_i}$. Taking the difference between the two distributions we have

$$\Delta\log(k_i) \sim N\left(\log(k_{\mathrm{best\,fit}_i}) - \log(k_{\mathrm{true}_i}), \sigma^2_{\mathrm{rxn}_i} + \sigma^2_{\mathrm{model}_i}\right) \quad (12)$$

giving us the distribution for $\Delta\log(k_i)$. However, this expression isn't very useful. We can roughly estimate $\sigma^2_{\mathrm{rxn}_i}$, but the other parameters are unknown and since this distribution is specific to reaction i we cannot draw samples from the node to estimate the parameters. It does, however, outline two primary sources of error in the quantity: limitations in the models ability to represent the chemical space and the errors in the training data. In general we expect there to be two limits. At lower nodes there will be fewer training reactions, but a much smaller chemical space. In this small chemical space limit we have $k_{\mathrm{best\ fit}_i} \approx k_{\mathrm{true}_i}$ and since the smaller chemical space is easier to fit with proper weighting we expect $\sigma^2_{\mathrm{model}_i}$ to be reaction independent and small giving us

$$\Delta\log(k_i) \sim N\left(0, \sigma^2_{\mathrm{rxn}_i} + \sigma^2_{\mathrm{model}}\right) \quad (13)$$

a dramatically simpler expression where $\sigma^2_{\mathrm{model}}$ is the reaction independent model variance. In this limit because the mean is zero we expect the rule to be more accurate than the individual training reactions used to fit it. In this case we can take advantage of the fact that

$$\frac{\Delta\log(k_i)}{\sqrt{\sigma^2_{\mathrm{rxn}_i} + \sigma^2_{\mathrm{model}}}} \sim N(0, 1) \quad (14)$$

and compute $\sigma^2_{\mathrm{model}}$ by solving

$$E\left[\frac{\Delta\log(k_i)}{\sigma^2_{\mathrm{rxn}_i} + \sigma^2_{\mathrm{model}}}\right] = 0 \quad (15)$$

However, this approach requires us to separate the small $\sigma^2_{\mathrm{model}}$ from large values of $\sigma^2_{\mathrm{rxn}_i}$. If high accuracy values for $\sigma^2_{\mathrm{rxn}_i}$ are available this is possible to do accurately. However, in this work we do not have sufficiently accurate values for $\sigma^2_{\mathrm{rxn}_i}$ and to ensure our estimates are reasonable we estimate all uncertainties in the other limit. This will likely cause overestimation of uncertainties at nodes that have very low uncertainties.

In the other limit at higher nodes there will be more training reactions and a larger chemical space. In this case we expect $\log(k_{\mathrm{best\ fit}_i}) - \log(k_{\mathrm{true}_i})$ to be large. In this case we expect the errors in k_{model_i} to dominate. This allows us to neglect $\sigma^2_{\mathrm{rxn}_i}$, although they are still necessary to use as weights. Note that when errors are properly weighted the true scale of $\sigma^2_{\mathrm{rxn}_i}$ is determined by the smallest value among the set of reactions. In this case however the simplification only gets us to

$$\Delta\log(k_i) \sim N\left(\log(k_{\mathrm{best\,fit}_i}) - \log(k_{\mathrm{true}_i}), \sigma^2_{\mathrm{model}_i}\right) \quad (16)$$

to get a distribution we can sample we have to assume there is a general non-reaction dependent $\sigma^2_{\mathrm{model}}$ associated with the chemical space and likely a small bias μ_{model} giving us

$$\Delta\log(k_i) \sim N(\mu_{\mathrm{model}}, \sigma^2_{\mathrm{model}}) \quad (17)$$

note that this analysis turns a lot of the bias error for individual reactions ($\log(k_{\mathrm{best\ fit}_i}) - \log(k_{\mathrm{true}_i})$) into an overall variance $\sigma^2_{\mathrm{model}}$. These limits are best differentiated by the criterion

$$\frac{\sigma^2_{\mathrm{model}}}{\sigma^2_{\mathrm{rxn\,min}}} \gg 1 \quad (18)$$

where $\sigma^2_{\mathrm{model}}$ is the model variance in the large chemical space limit and $\sigma^2_{\mathrm{rxn\ min}}$ is the variance of the most accurate training reaction matching the node. If the criterion is true it is best to use the large chemical space approach if $\frac{\sigma^2_{\mathrm{model}}}{\sigma^2_{\mathrm{rxn\,min}}} \sim 1$ or smaller it is best to use the small chemical space approach. Although as noted above we do not have sufficiently accurate training uncertainties to accurately implement the small chemical space approach. Our implementation of the large chemical space approach is described below.

First, we estimate the distribution of errors in the training data. Training reactions within the RMG-database come from many different sources. However, the vast majority are based on quantum chemistry calculations. Rate expressions from quantum chemistry calculations primarily have four sources of error: errors in the computed frequencies, errors in the internal rotor treatment, errors in the computed energies and errors in fitting the rate coefficients to a functional form (*e.g.* Arrhenius equation). While the fourth is commonly reported because it is easiest to estimate it is rarely significant. The errors are most often dominated by the error in the computed energies. While one could envision complex schemes of accounting for calculation uncertainties typically only the level of theory is recorded in the RMG-database. For this reason we map RMG-database reactions' ranks

(identifiers associated with source types: experiments, calculations, and estimates) to our own estimates of 2-sigma uncertainties in the Arrhenius E_a. For example a CBS-QB3 calculated rate (a typical level of theory in the RMG training data) would be associated with a 2.5 kcal mol^{-1} uncertainty while the least reliable data source, a "rule of thumb" generalization, would be assigned a 14 kcal mol^{-1} uncertainty.[47] We express our errors as $\Delta\log(k)$ rather than Δk because $\Delta\log(k) \sim \Delta E_a$.

Once we have estimates of the uncertainties in the training data, we can look at estimating the uncertainties in the predictions of our new tree-based rate estimator. For similar reasons to building the tree we do this analysis at 1000 K. However, under suitable assumptions (for example all of the error being associated with E_a) it is relatively easy to reasonably extrapolate the uncertainties generated to other temperatures. For each node with more than one training reaction we compute the leave-one-out errors for the model predictions for reactions that match that node against the training reactions at 1000 K.

$$\Delta\mathrm{Log}(k_i) = \mathrm{Log}\left(\frac{k_{\mathrm{model(rxns}-i)}}{k_i}\right) \tag{19}$$

where $k_{\mathrm{model(rxns}-i)}$ is the prediction of the model without training reaction i and k_i is training reaction i. We compute the variance in the training data assuming the error is associated with E_a

$$\frac{1}{w_i} = \sigma^2_{\mathrm{rxn}_i} = \left(\frac{\sigma_{E_i}}{RT_{\mathrm{ref}}}\right)^2 \tag{20}$$

where σ_{E_i} is the standard deviation in the E_a of the ith training reaction calculated from the rank errors, σ_{rxn_i} is the standard deviation in $\log(k_i)$, R is the gas constant and T_{ref} is the reference temperature. Weighting each leave-one-out error by the expected uncertainty in the data point due to how its E_a was computed, we compute the weighted mean model error μ_{model}

$$\mu_{\mathrm{model}} = \frac{\boldsymbol{w}\cdot\Delta\mathbf{Log}(\boldsymbol{k})}{\sum_i w_i} \tag{21}$$

which one might expect to be small for nodes with a large number of training reactions if the leave-one-out errors are equally likely to be positive or negative. The weighted variance of the leave-one-out prediction errors can also be obtained in this manner

$$\sigma^2_{\mathrm{model}} = \frac{\left(\boldsymbol{w}\cdot\left(\Delta\mathbf{Log}(\boldsymbol{k}) - \mu_{\mathrm{model}}\right)^2\right)}{\sum_i w_i - \frac{\sum_i w_i^2}{\sum_i w_i}} \tag{22}$$

where σ_{model} is the standard deviation in the model estimate of $\log(k)$. In general $\sigma^2_{\mathrm{model}}$ is expected to be large when $\Delta\mathbf{Log}(\boldsymbol{k}) - \mu_{\mathrm{model}}$ is large because the chemical space is large and/or training reactions are inaccurate, and when N_{rxns}, the number of training reactions, is small. $\sigma^2_{\mathrm{model}}$ will be small when $\Delta\mathbf{Log}(\boldsymbol{k}) - \mu_{\mathrm{model}}$ is small because the chemical space is small or training reactions are accurate, and asymptote down to a constant value when N_{rxns} is large. We also define

$$\mu_{\mathrm{data}_m} = \frac{\sum_i^{N_{\mathrm{rxns}_m}} \mathrm{Log}(k_i)}{N_{\mathrm{rxns}_m}} \tag{23}$$

where μ_{data_m} is the mean of the data at node m and N_{rxns_m} is the number of training reactions at node m. Taking the difference between a parent and one of its child nodes $\mu_{\mathrm{data}_{\mathrm{parent}}} - \mu_{\mathrm{data}_{\mathrm{child}}}$ provides us with some measure of whether the chemical space spanned by the child is representative of the parent. If this number is small in magnitude the node may be better represented by the parent that will have more training reactions to fit to, if it is large in magnitude the parent is likely a poor representation. In addition to μ_{model}, σ_{model} and μ_{data_m} we also provide the number of reactions it was fit to and the name of the node, which is important for accounting for correlation between uncertainties.[45]

We now have the capability to estimate reaction rate coefficients and uncertainties (based on μ_{model} and $\sigma^2_{\mathrm{model}}$) at each node. This in fact provides us with many different estimates for a given $k(T)$: one for each node in the tree a reaction matches. Naively one might think it would be best to estimate each reaction using the most specific node it matches, however, this is not always the case. At each node there is error associated with ability of the Blowers–Masel model to accurately represent all the reactions at that node, the error in the training reactions, and also error associated with the ability to accurately estimate the Blowers–Masel parameters from the available training reactions. At nodes near the top of the tree there are many reactions making it possible to accurately calculate the Blowers–Masel parameters, however, the chemical space spanned can be quite large making it difficult for a single Blowers–Masel model to represent all of the involved reactions. At nodes near the bottom of the tree the chemical space spanned is much smaller and the Blowers–Masel model can better represent the space, but there are fewer reactions to fit to making the Blowers–Masel fit sensitive to errors in the training data.

Now that we have uncertainties it is possible to use them to choose the best node to estimate from. If we think an estimate from a certain node is less accurate than estimating from its parent we can estimate from its parent instead. However, this analysis needs to balance several different kinds of error: the error expected from the model at that node, the error expected from the model at the parent node, and the error associated with using the parent node to estimate at the child node. The later may seem unimportant, but it's a very important consideration particularly in the dataset we use. This is because rate rules especially at large scale are manually constructed to generate accurate chemical kinetic models. This means that a sensitive reaction may be similar to many training reactions in the database, while an

insensitive reaction may only be similar to one or two. This means we may have cases where moving up a node dramatically changes estimates. To account for these errors we add the difference in the data mean values of the distributions to the bias (model mean) of the parent distribution. Assuming errors in $\log(k)$ are distributed normally and given that for a half-normal distribution the expected value is $\sqrt{\frac{2\sigma^2}{\pi}}$ we can compare the expected errors. Taking an upper bound on the means gives us the criterion

$$|\mu_{\text{model}_{\text{node}}}| + \sqrt{\frac{2\sigma^2_{\text{model}_{\text{node}}}}{\pi}} > \left|\left(\mu_{\text{data}_{\text{parent}}} - \mu_{\text{data}_{\text{node}}}\right) - \mu_{\text{model}_{\text{parent}}}\right| + \sqrt{\frac{2\sigma^2_{\text{model}_{\text{parent}}}}{\pi}} \quad (24)$$

where node and parent denote the uncertainty distribution properties associated with each node. If eqn (24) is true it is better to use the parent node when estimating $k(T)$ and uncertainties. In most cases $\mu_{\text{model}_{\text{node}}}$ and $\mu_{\text{model}_{\text{parent}}}$ are small relative to the other terms. Near the top of the tree when many training reactions are available accuracy is limited by the fact that the Blowers–Masel cannot represent the set of reactions well and we expect that $\sigma_{\text{model}_{\text{node}}} < \sigma_{\text{model}_{\text{parent}}}$ and that $\mu_{\text{data}_{\text{parent}}} - \mu_{\text{data}_{\text{node}}}$ is large in magnitude implying that reactions are better estimated by child nodes if they match them. Near the bottom of the tree where there are fewer training reactions accuracy is limited by the quantity and quality of training reactions and usually $\sigma_{\text{model}_{\text{node}}} > \sigma_{\text{model}_{\text{parent}}}$ so often reactions are better estimated at the parent nodes. However, while typically $\mu_{\text{data}_{\text{parent}}} - \mu_{\text{data}_{\text{node}}}$ will be smaller in this regime it can be very large when a segment of chemical space containing reactions with very different rate coefficients is only represented by a small number of training reactions making some reactions more accurately computed from a child than a parent.

In the literature there are arguments that rate coefficient errors should be treated log-uniformly instead of log-normally.[48] However, in practice we found when attempting to represent larger normal distributions based on small samples (2–4 data points) that treating these samples as distributed normally significantly improved agreement with the histograms over uniform when the samples were fairly representative and was roughly equally as bad as treating them uniform when they were not. However, this assumption is only made for purposes of ascending the tree during rate estimation and our uncertainty outputs are of course not distribution specific.

2.8 Regularization and embedding qualitative chemical knowledge in estimators

Fundamentally regularization is choosing between two different estimators that have similar accuracy on the data they were trained on.[41] It is an important component in machine learning for avoiding overfitting or having a model that fits the training data well, but performs much more poorly on other data. In most contexts discussing the space of models with similar training accuracy is complex. However, for our subgraph isomorphic decision trees it is fairly simple.

Earlier we discussed that during tree generation we tracked specification extensions in each structure down the tree that matched all of the reactions matching that node. Suppose again we have the node R–C*$\overset{?}{-}$R and suppose our training reaction templates are CH_3–C*H_2–CH_2–CH_2–CH_3, CH_3–C*H_2–CH_2–OH and CH_3–C*H_2–CH_2–CH═O. It is clear here that converting R– > C for both R's in the node will not affect the training reactions that match this node and therefore not affect training errors. However, if we were to use this tree to estimate reactions represented by the templates H–C*H_2–CH_3 and CH_3–C*H_3 whether they matched the node and thus how they were estimated would be changed if one were to convert R– > C for those R's.

Typically a model would be regularized by setting aside a test set of reactions and then tuning optimization hyperparameters according to heuristics to improve performance on the test set. This is problematic for small datasets particularly when the estimators' accuracy may depend on the presence of key reactions in the training set. Here we can simply do so by moving along these "regularization" dimensions that do not affect the training split without sacrificing any accuracy on reactions similar to the training set.

Even more beautifully these regularization dimensions are human readable. This means that we can do more than just regularize while preserving training accuracy. An expert can embed their chemical knowledge within the estimator by adjusting the regularization algorithm. Suppose we have the node C*$\overset{?}{-}$R and we have training reaction templates: C*H_3–CH_2–CH_3, C*H_3–O–CH_3 and C*H_2═O. A good safe default regularization choice is to make each node as specific as the reaction set that matches it so you might get post regularization C*–$^?$ [C, O]. However, suppose the expert does not think the identify of that atom is important they could choose to keep that atom general or at least extend it to another atom type. This can be particularly helpful for small datasets.

The tree generation algorithm is even robust to mistakes on the part of the expert. In the last case if the identity of that atom is important you would expect the algorithm to extend the tree with C*–$^?$O or C*–$^?$C. The expert's choice of regularization won't affect estimation in the tree for any reaction hitting this split or below. This means that if enough data is present to learn the difference these substructures make on rate estimation any potential mistakes in the chemical knowledge embedded in the regularization will be ignored.

2.9 Performance and scaling

If our generated tree was a binary tree with perfectly even splits we would expect to have the number of nodes double

until we had N_{rxns} nodes. The partial sum for the number of nodes in this idealized tree with k layers is $2^{k+1} - 1$ since our last layer is $2^k = N_{rxns}$ this implies that our number of nodes should be approximately $2N_{rxns}$, which agrees well with observed tree node numbers, and scales, $O(N_{rxns})$, linearly with our number of reactions. However, the amount of work needed for each node can vary significantly, but has two primary expensive operations: making new groups which scales $O(N_{extensions})$ and identifying whether extensions map the reactions at the node which (noting that the number of reactions at a node scale with the total number of training reactions) scales $O(N_{node\ rxns}N_{extensions})$, where $N_{node\ rxns}$ is the number of reactions at a node that scales linearly with N_{rxns} and $N_{extensions}$ is the number of extensions generated at a node. This means that for large enough N_{rxns} the overall naive algorithm will scale quadratically with N_{rxns}.

In practice the algorithm works quite efficiently serially on datasets that tend to have low numbers of heavy atoms or are small. For these datasets training times using the naive algorithm are at most an hour. This heavy atom dependence comes from its impact on $N_{extensions}$. Larger numbers of heavy atoms make it possible to have nodes where all the reactions involve large species that are nearly identical around the reactive sites. In these extension generation cases $N_{extensions}$ can combinatorically explode from repeatedly generating bond extensions that need to be extended themselves resulting in $N_{extensions}$ being several orders of magnitude larger than is typical. This becomes problematic for a couple of RMG families that contain 3000–6000 reactions a significant subset of which have many heavy atoms.

Fitting the Blower–Masel interpolants could also be limiting in the overall process of generating an estimator. Fitting an interpolant scales roughly $O(N_{rxns})$ so naively running the fitting at every node will scale roughly quadratically. However, one can set a maximum number of reactions N_{max} and using stratified sampling based on rate values at a chosen temperature to select a representative subset of N_{max} reactions to fit to. Fitting on this subset of reactions is O(1) making the overall fitting process scale linearly with the number of reactions. However, we have not found this process to be limiting in practice so this approach is not implemented here.

We have developed techniques that enable parallelization of tree generation, avoid computational explosion in extension generation and enable linear scaling with respect to N_{rxns}.

2.9.1 Parallelization. The two dominant processes in estimator training are the construction of the tree and the fitting of the Blower–Masel interpolants. The later process is embarrassingly parallel so we will focus on discussing the structure of the former.

The construction of subtrees that don't intersect with each other is embarrassingly parallel, but are dependent on the shared nodes above. The parallelization is handled recursively. Processes have an assigned subtree and a specific number of processors at their disposal. If a split divides the set of reactions into large enough chunks that it is worth sending information to another processor it will generate a subprocess that is assigned an associated subtree in the split and an appropriate number of processors for the size of that subtree. When a process completes its subtree it sends the subtree back to the process that spawned it and so on until the entire tree is constructed.

2.9.2 Cascade algorithm. Unfortunately, a lot of time is spent generating the top nodes of the tree before parallelization can be properly taken advantage of. This is because if a tree has 3000 reactions at the top node the algorithm needs to run subgraph isomorphism checks between each proposed extension and 3000 reactions instead of perhaps 10 reactions further down the tree and occurs because of the aforementioned quadratic scaling. However, the top nodes are identifying the substructures that most affect the rate across the whole set of reactions. These particular substructures should be identifiable from a smaller

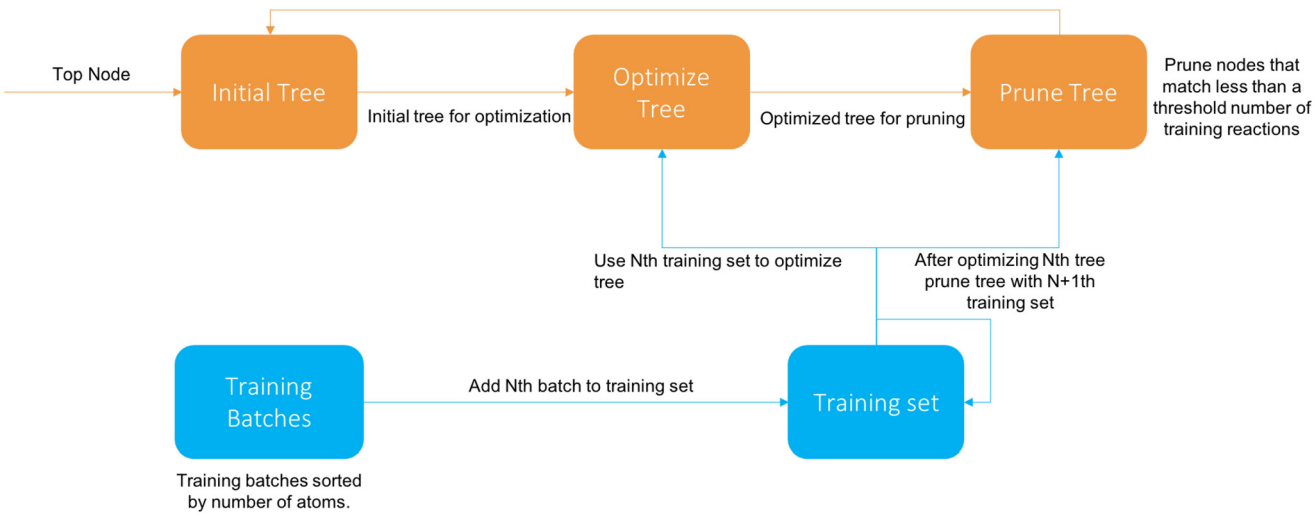

Fig. 4 Diagram of cascade algorithm.

Table 1 Comparison of accuracy of RMG rate rules (RR) and the subgraph isomorphic decision tree (SIDT) estimator for three different RMG families oxygen substitution (O-Sub), intra-molecular hydrogen transfer (intra-H), internal endocyclic radical addition (Int-Endo) and radical addition (R-Add)

Estimator	O-Sub RR	O-Sub SIDT	Intra-H RR	Intra-H SIDT	Int-Endo RR	Int-Endo SIDT	R-Add RR	R-Add SIDT	H-Abs RR	H-Abs SIDT
Median absolute error factor	10.3	5.28	8.94	3.56	9.67	1.73	2.25	1.88	5.11	4.05
MAE factor	18.5	10.1	38.1	10.9	24.7	2.95	3.07	2.34	16.4	8.02
RMSE factor	61.7	27.6	575	79.3	98.3	7.07	5.59	3.51	89.7	23.7
2-Sigma error factor	3876	770	333 000	6320	9710	50.1	31.3	12.3	8040	564

Table 2 Reaction templates

Oxygen substitution	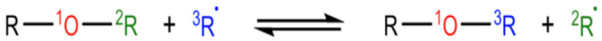
Intra-molecular hydrogen transfer	
Internal endocyclic radical addition	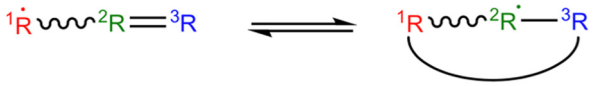
Radical addition	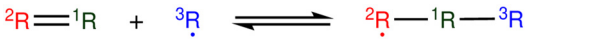
Hydrogen abstraction	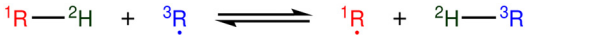

training set particularly ones with simpler reactants. Furthermore, if we can effectively bound the size of the training set being used to test extensions the algorithm will scale linearly with N_{rxns}.

The cascade algorithm operates on the principle that we feed data to the training algorithm as needed to extend the tree properly instead of all at once. A diagram of the algorithm is available in Fig. 4.

We first sort the reactions based on their number of atoms and divide them into batches of a specified size. The first iteration the tree is trained on the first batch like normal. After the Nth tree generation the N + 1th batch (if it exists) is added and descends down the tree. Then the tree is pruned, removing all nodes that have more than a set fraction of reactions from the latest batch, and then reoptimized with the new reactions. Once there are no batches left it terminates after optimization.

2.9.3 Extension generation adjustments. Since the primary bottleneck is in extension generation it makes sense to examine ways to reduce the amount of work that needs done during this step. There are a lot of different ways this might be done and this choice is mostly about picking the approach that provides the most speed up while decreasing accuracy as little as possible. We approached this by capping the number of recursions extension generation is allowed to do if a splitting extension has already been found and additionally capping the number of extensions allowed in a recursion.

Normally if a bond formation extension matches all reactions the resulting structure is sent to be extended itself. This ensures that every set of reactions can be split. However it is very expensive because computing extensions for each new structure is roughly as expensive as the original extension generation step and the number of extensions has a tendency to combinatorically explode. Even worse, unless these extensions are linking back to another reaction site or forming a ring they typically won't have much of an affect on the reaction rate. This means they won't be picked and will likely end up regenerated entirely when extensions are generated a level down the tree.

We added the ability to cap the recursion depth for extension generation as long as a splitting extension has already been found. Tests capping the depth at one recursion on intra-molecular hydrogen transfer actually showed a small, but measurable decrease in error (except for median error that increased by only a factor 1.04) suggesting this has relatively minimal impact on accuracy.

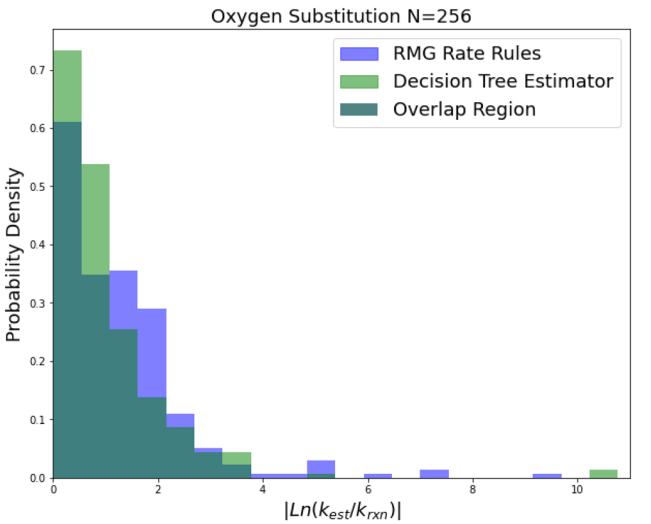

Fig. 5 Histogram of errors for oxygen substitution reactions. Dark green is overlap. Trained on 256 reactions.

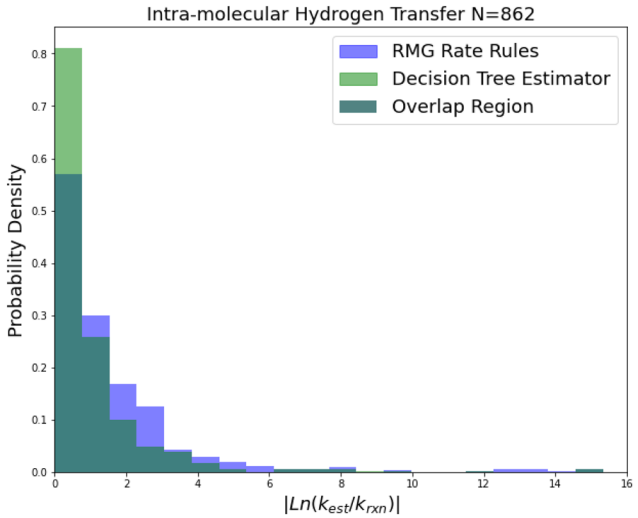

Fig. 6 Histogram of errors for intra-molecular hydrogen transfer reactions. Dark green is overlap. Trained on 422 reactions.

We also added the ability to end splitting attempts if the recursion is returning more than a set number of extensions. This robustly prevents combinatoric explosion. One can certainly contrive counter examples where this choice might be problematic. However, in practice with a cap of 100 extensions this has only been observed to affect nodes with only two reactions present.

3 Results and discussion

3.1 Rate estimation

Estimators were generated using the training sets for RMG's oxygen substitution, intra-molecular hydrogen transfer, internal endocyclic radical addition, radical addition and hydrogen abstraction families. These reaction families were chosen primarily because they have larger training sets and higher variances in their rate coefficients. On Github, the associated database state is available on the sidt_paper branch of the RMG-database and the associated code state used is available on the sidt_paper branch of RMG-Py. All of these except internal endocyclic radical addition and radical addition are their own reverse and the reversed reactions were used as a part of the training set. Note that we count these reversed reactions when giving the number of reactions in the training set. The templates for these reactions are available in Table 2.

All RMG families tested except for hydrogen abstraction and radical addition were trained on the vanilla algorithm capping the number of recursions at two and capping the number of recursion items at 100 in less than two hours. Hydrogen abstraction and radical addition were both trained in less than 7 hours using the cascade algorithm with a batch size of 1000, a reoptimization fraction of 0.25 and fitting the interpolants in parallel on six cores. The default regularization scheme was used for all families.

Reaction family error factors based on leave-one-out cross validation are available in Table 1. Histograms of leave-one-out errors are available in Fig. 5–8. The subgraph isomorphic decision tree (SIDT) estimator is a significant improvement over RMG's RR scheme in every category for every reaction family and in a number of cases approaches the dataset error limits. We can see both significant improvements in the estimation of reactions RR already predicts well and very large improvements in the estimation of reactions not predicted well by RR. Differences in prediction performance on different reaction families are best understood as result of different overall variances in the rate coefficient values, different quantities of training reactions, different training reaction accuracies and different overall chemical scopes.

Oxygen substitution is a particularly useful test case because the training set is entirely CBS-QB3 calculations. In

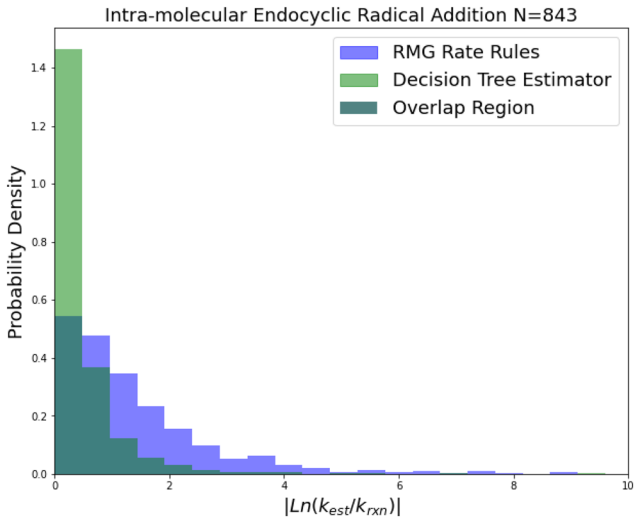

Fig. 7 Histogram of errors for intramolecular endocyclic radical addition reactions. Dark green is overlap. Trained on 843 reactions.

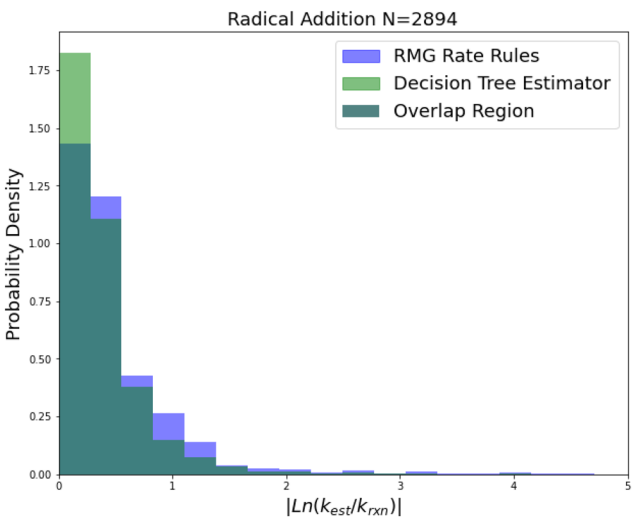

Fig. 8 Histogram of errors for radical addition reactions. Dark green is overlap. Trained on 2892 reactions.

this case the improvement is pretty consistent: about a factor of 2–5 in all errors. Given that the median absolute error achieved by SIDT is 5.28, which corresponds to roughly 3.34 kcal mol^{-1} in terms of energy, and the training set assuming a lognormal distribution only has a median absolute error of about 0.84 kcal mol^{-1} this set provides a good idea of performance improvement away from the training set limit. It also shows the performance of this method on small training sets.

Intra-molecular hydrogen transfer is a reaction family of more practical interest than oxygen substitution. The training set is mostly CBS-QB3 calculations, but integrates some DFT calculations and literature estimates. The accuracy improvements mostly decrease for this family across 2-sigma errors, RMSE errors, MAE errors to median absolute errors implying that the accuracy improvements on reactions not predicted well by RR are much larger than those for reactions that are predicted well by RR.

Internal endocyclic radical addition is another important reaction family and is one of RMG's larger families with 843 reactions. The training reactions are mostly CBS-QB3 calculations, with a handful of G3 calculations and literature estimates. An enormous improvement in estimation for this family is visible in Fig. 7. The 2-sigma improvement is larger than the other improvements this time as well (~190×), but the improvement is more consistent across the other metrics. Impressively the median absolute error for this family in terms of energy corresponds to 1.09 kcal mol^{-1} while the training set median absolute error assumed all CBS-QB3 calculations should be about 0.84 kcal mol^{-1}. This amounts to about a 10% error against the training set at 1000 K. This suggests that there is little room for improvement over the SIDT estimator on the best-estimated 50% of reactions in this family.

Radical addition is an important reaction family and this is reflected in the size of its 2892 reaction training set. This training set however is mostly estimates based on a reaction group additivity scheme, except for about 400 reactions that are mostly calculations at the CBS-QB3 level of theory or better. However, it is clear that these estimates must at least have low uncorrelated errors because once again we can see that SIDT is achieving a median accuracy of 1.25 kcal mol^{-1} not much larger than the 0.88 kcal mol^{-1} limit of a pure CBS-QB3 dataset. The associated histograms are available in Fig. 8. While the improvements for this family are smaller this seems likely to be a result of the fact that the accuracy of this family is being limited by the quality of the training data.

Hydrogen abstraction is another important reaction family. Much like radical addition the training set is mostly estimates from a group additivity scheme along with CBS-QB3 or better calculations and some estimates. The comparison histogram is available in Fig. 9. The improvements are more similar to those in intra-molecular hydrogen transfer being greatest for 2-sigma error and

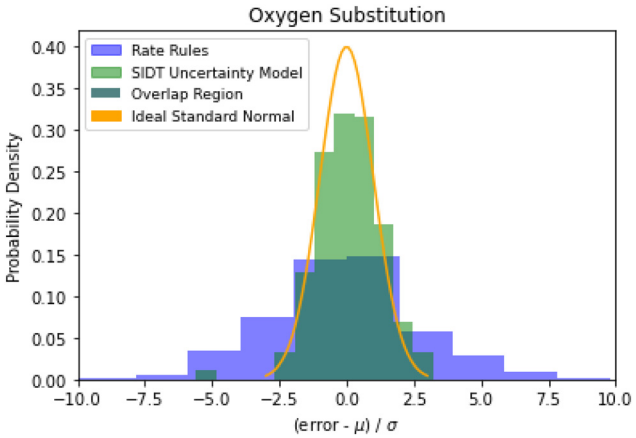

Fig. 10 Histogram of normalized errors for the oxygen substitution reactions. The uncertainties in rate rules (purple) are taken from Gao *et al.* 2020.[45] Ideally at high sample sizes the histogram should become a normal distribution.

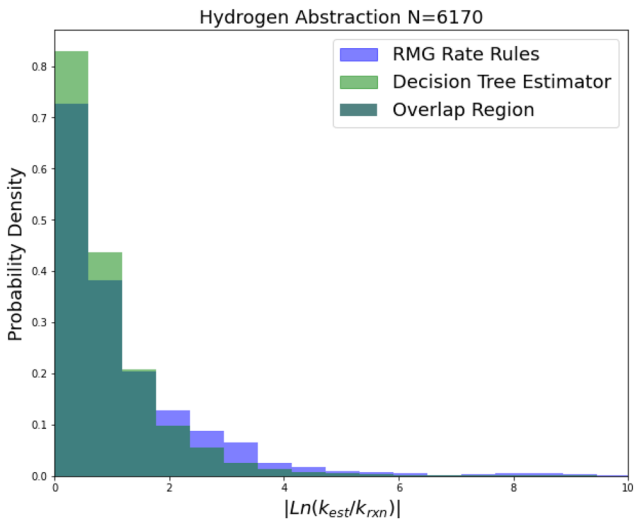

Fig. 9 Histogram of errors for bimolecular hydrogen abstraction reactions. Dark green is overlap. Trained on 6170 reactions.

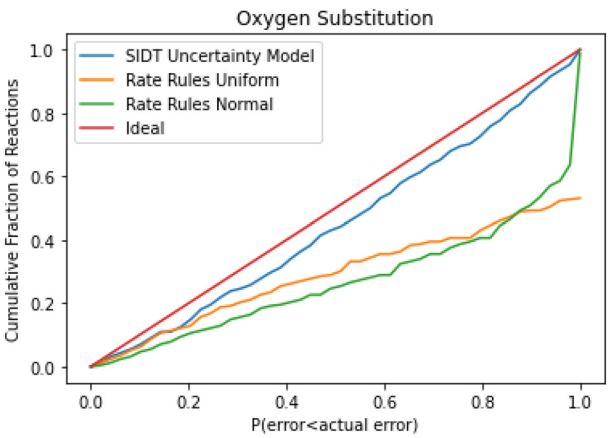

Fig. 11 Cumulative histogram of the probability that the uncertainty estimate is less than the actual leave-one-out error. The rate rules uncertainties are from Gao *et al.* 2020 and both uniform and normally distributed uncertainty models from that work are included. The new SIDT method (blue) slightly underestimates the true errors by this measure.

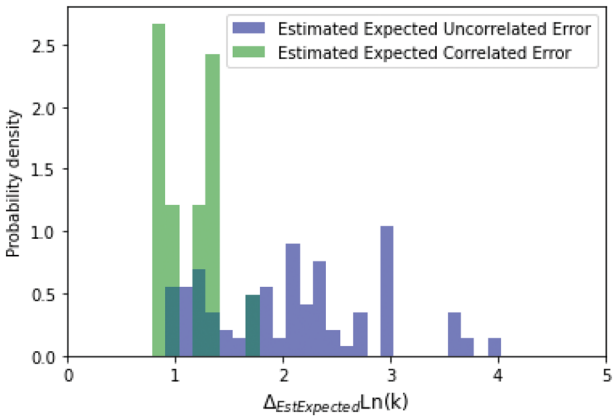

Fig. 12 Histogram of expected correlated and uncorrelated errors for oxygen substitution reactions.

Table 3 Mean and standard deviation of the normalized errors for the SIDT uncertainties. The ideal values are 0.0 and 1.0 respectively

Reaction class	O-Sub	Intra-H	Int-Endo	R-Add	H-Abs	Ideal
Mean	0.09	0.14	−0.08	0.21	0.03	0.0
Std	1.21	1.48	1.47	1.04	1.19	1.0

gradually decreasing across RMSE error, MAE error and median absolute error. However, in general the lower median accuracy for both RR and SIDT and the low improvement in median accuracy relative to the other smaller families suggests that either the training set is less accurate or the estimation problem is simply more difficult for hydrogen abstraction.

3.2 Uncertainty estimation

Examining the accuracy of uncertainties is significantly more difficult than that of predictions. A histogram of errors in $\log(k(1000\ \mathrm{K}))$ normalized by their uncertainty distribution parameters is available in Fig. 10. The SIDT uncertainty estimates approach the ideal standard normal distribution much closer than the heuristical uncertainties from Gao *et al.* 2020.[45] Here the SIDT is able to achieve a mean and standard deviation of 0.09 and 1.21 respectively compared to −0.172 and 3.30 from the heuristics.

A cumulative histogram of the probability of errors is available in Fig. 11. This plot is a bit more difficult to interpret. Uncertainty models above the red "ideal" line are overpredicting the uncertainties while those under the line are underpredicting uncertainties. Along the *x*-axis the histogram is excluding reactions with larger and larger errors normalized by their predicted uncertainty. From this plot we can conclude that while

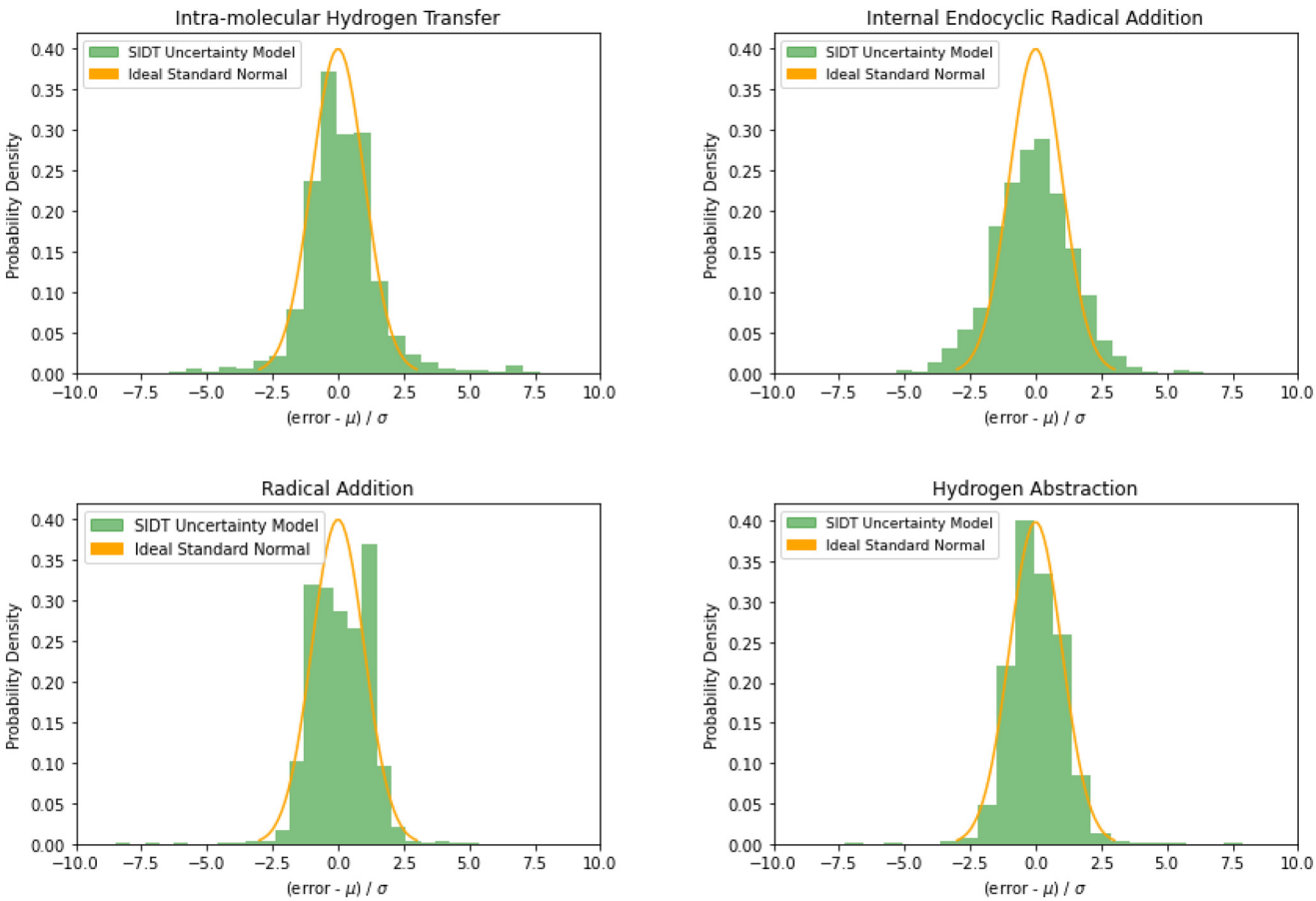

Fig. 13 Histograms of normalized errors. Ideally at high sample sizes the histogram should match the standard normal density function.

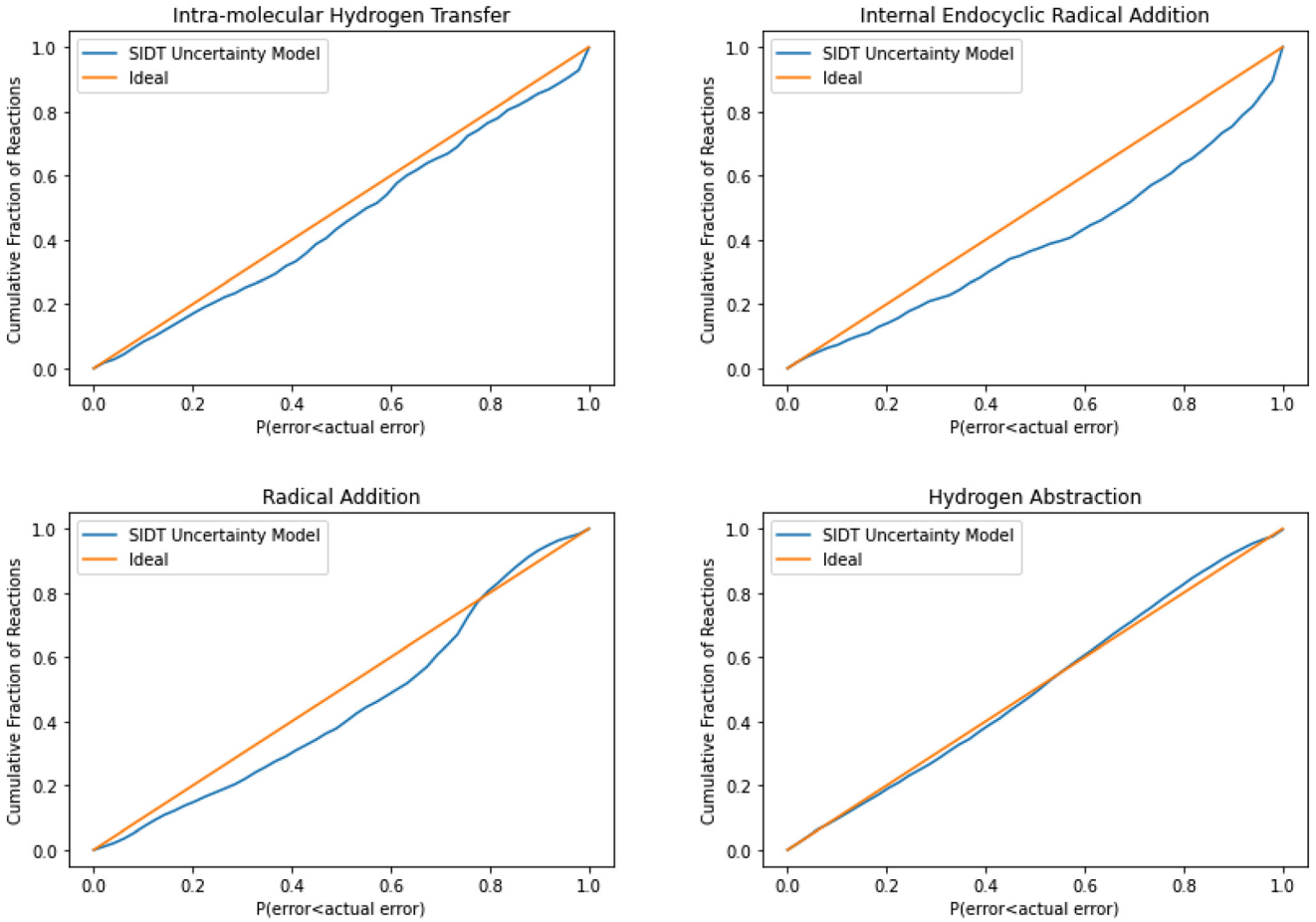

Fig. 14 Cumulative histogram of the probability that the uncertainty estimate from SIDT is less than the actual leave-one-out error.

all methods underpredict uncertainties in this family the SIDT uncertainty model underpredicts by significantly less than the heuristics from Gao *et al.* 2020.[45]

A histogram of the expected correlated and uncorrelated errors for oxygen substitution reactions is shown in Fig. 12. As one might expect for a tree-based estimator, some of the errors are correlated and some uncorrelated.

The normalized error results for SIDT for the other reaction classes are available in Table 3 and Fig. 13. All of the reaction classes have normalized standard deviations under 1.5, however, the larger families (radical addition and hydrogen abstraction) achieve values much closer to 1.0. The cumulative histograms for SIDT for the other reaction classes are available in Fig. 14. While the error estimates for intramolecular hydrogen transfer and bimolecular hydrogen abstraction reactions are close to ideal the SIDT often underestimates the true uncertainties for bimolecular radical addition and intramolecular endocyclic radical addition reactions.

4 Conclusions

We have presented a machine learning based estimator automatically trainable from an arbitrary set of reactions. This estimator is highly scalable from very small to large dataset sizes and is easy to update. In spite of the use of machine learning the estimator is equally human readable and human manipulable as the RR scheme it is compared against. It can naturally embed qualitative chemical knowledge from experts to improve estimation. Additionally, it incorporates accurate uncertainty estimation and provides properties of the uncertainty distribution that enable the information to be used in many contexts. The SIDT estimator has demonstrated significant accuracy improvements over the state of the art in most cases and measures and has been demonstrated to approach the accuracy limits of the dataset in some cases.

While the presented technique learns reaction rates that occur as a function of specific sites on a molecule, the SIDT approach is relatively easy to extend to whole molecule properties. One simply needs to define an appropriate summation scheme and interpolant, a new objective function, and a technique for picking which nodes to extend first (as unlike in the current scheme the order in which nodes are extended may matter). The remaining machinery remains the same.

As we look forward to the future of kinetics and other property estimators it is important to keep in mind the needs

of mechanism builders and the kinetics community as a whole. Having high accuracy today is convenient, but even more important is the ability to easily improve and extend the estimator in the future. The method presented here provides the user with uncertainty estimates to help determine what can be and needs to be improved, human readability to determine how to improve the estimator, and scalability and automatic training to easily update the estimator. We hope to provide a new standard for what mechanism builders should expect from their property estimators.

Conflicts of interest

There are no conflicts to declare.

Acknowledgements

This material is based upon work supported by the U.S. Department of Energy's Office of Energy Efficiency and Renewable Energy (EERE) under Award Number DE-EE0007982 (Co-Optima). This research was supported by the Exascale Computing Project (ECP), Project Number: 17-SC-20-SC, a collaborative effort of two DOE organizations, the Office of Science and the National Nuclear Security Administration, responsible for the planning and preparation of a capable exascale ecosystem including software, applications, hardware, advanced system engineering, and early test bed platforms to support the nation's exascale computing imperative.

Notes and references

1 M. S. Johnson, M. R. Nimlos, E. Ninnemann, A. Laich, G. M. Fioroni, D. Kang, L. Bu, D. Ranasinghe, S. Khanniche, S. S. Goldsborough, S. S. Vasu and W. H. Green, *Int. J. Chem. Kinet.*, 2021, **53**, 915–938.

2 M. Liu, A. G. Dana, M. S. Johnson, M. J. Goldman, A. Jocher, A. M. Payne, C. A. Grambow, K. Han, N. W. Yee, E. J. Mazeau, K. Blondal, R. H. West, C. F. Goldsmith and W. H. Green, *J. Chem. Inf. Model.*, 2021, **61**, 2686–2696.

3 M. S. Johnson, X. Dong, A. G. Dana, Y. Chung, J. D. Farina, R. J. Gillis, M. Liu, N. W. Yee, K. Blondal, E. Mazeau, C. A. Grambow, A. M. Payne, K. A. Spiekermann, H.-W. Pang, C. F. Goldsmith, R. H. West and W. H. Green, *J. Chem. Inf. Model.*, 2022, **62**, 4906–4915.

4 C. W. Gao, J. W. Allen, W. H. Green and R. H. West, *Comput. Phys. Commun.*, 2016, **203**, 212–225.

5 R. G. Susnow, A. M. Dean, W. H. Green, P. Peczak and L. J. Broadbelt, *J. Phys. Chem. A*, 1997, **101**, 3731–3740.

6 J. Zador and J. A. Miller, *Proc. Combust. Inst.*, 2015, **35**, 181–188.

7 P. L. Bhoorasingh, B. L. Slakman, F. Seyedzadeh Khanshan, J. Y. Cain and R. H. West, *J. Phys. Chem. A*, 2017, **121**, 6896–6904.

8 G. Henkelman, B. P. Uberuaga and H. Jonsson, *J. Chem. Phys.*, 2000, **113**, 9901–9904.

9 M. S. Johnson, M. Gierada, E. D. Hermes, D. H. Bross, K. Sargsyan, H. N. Najm and J. Zador, *J. Chem. Inf. Model.*, 2023, **63**, 5168.

10 P. Zimmerman, *J. Chem. Theory Comput.*, 2013, **9**, 3043–3050.

11 S. Maeda, T. Taketsugu and K. Morokuma, *J. Comput. Chem.*, 2014, **35**, 166–173.

12 Y. V. Suleimanov and W. H. Green, *J. Chem. Theory Comput.*, 2015, **11**, 4248–4259.

13 A. G. Dana, D. Ranasinghe, O. H. Wu, C. Grambow, X. Dong, M. S. Johnson, M. Goldman, M. Liu and W. H. Green, *ARC – Automated Rate Calculator*, **https://github.com/ReactionMechanismGenerator/ARC**.

14 S. N. Elliott, K. B. Moore, A. V. Copan, M. Keceli, C. Cavallotti, Y. Georgievskii, H. F. Schaefer and S. J. Klippenstein, *Proc. Combust. Inst.*, 2021, **38**, 375–384.

15 C. A. Grambow, A. Jamal, Y.-P. Li, W. H. Green, J. Zador and Y. V. Suleimanov, *J. Am. Chem. Soc.*, 2018, **140**, 1035–1048.

16 S. Maeda and Y. Harabuchi, *J. Chem. Theory Comput.*, 2019, **15**, 2111–2115.

17 C. A. Grambow, L. Pattanaik and W. H. Green, *J. Phys. Chem. Lett.*, 2020, **11**, 2992–2997.

18 K. Spiekermann, L. Pattanaik and W. H. Green, *Sci. Data*, 2022, **9**, 1–12.

19 L. Pattanaik, *PhD thesis*, Massachusetts Institute of Technology, 2023.

20 K. A. Spiekermann, L. Pattanaik and W. H. Green, *J. Phys. Chem. A*, 2022, **126**, 3976–3986.

21 O.-E. Ganea, C. W. Coley, R. Barzilay, K. F. Jensen, W. H. Green and T. S. Jaakkola, *Advances in Neural Information Processing Systems*, 2021, vol. 34, pp. 13757–13769.

22 E. Heid and W. H. Green, *J. Chem. Inf. Model.*, 2022, **62**, 2101–2110.

23 S. W. Benson and J. H. Buss, *J. Chem. Phys.*, 1958, **29**, 546–572.

24 R. Van de Vijver, M. K. Sabbe, M.-F. Reyniers, K. M. Van Geem and G. B. Marin, *Phys. Chem. Chem. Phys.*, 2018, **20**, 10877–10894.

25 H. H. Carstensen and A. M. Dean, *J. Phys. Chem. A*, 2009, **113**, 367–380.

26 R. Sumathi and W. H. Green, *J. Phys. Chem. A*, 2002, **106**, 5474–5489.

27 R. H. West, J. W. Allen and W. H. Green, *ChemInform*, 2012, **43**(36), DOI: **10.1002/chin.201236258**.

28 M. Saeys, M.-F. Reyniers, V. Van Speybroeck, M. Waroquier and G. B. Marin, *ChemPhysChem*, 2006, **7**, 188–199.
29 J. W. Allen, *PhD thesis*, Massachusetts Institute of Technology, 2013.
30 S. Choi, Y. Kim, J. W. Kim, Z. Kim and W. Y. Kim, *Chem. – Eur. J.*, 2018, **24**, 12354–12358.
31 S. Datta, V. A. Dev and M. R. Eden, *Comput. Chem. Eng.*, 2017, **106**, 690–698.
32 D. L. Baulch, M. J. Pilling, C. J. Cobos, R. A. Cox, C. Esser, P. Frank, T. Just, J. A. Kerr, J. Troe, R. W. Walker and J. Warnatz, *J. Phys. Chem. Ref. Data*, 1992, **21**, 411–734.
33 M. Frenklach, A. Packard and P. Seiler, *Proc. Am. Control Conf.*, 2002, 4135–4140.
34 D. A. Sheen, X. You, H. Wang and T. Løvås, *Proc. Combust. Inst.*, 2009, **32I**, 535–542.
35 H. Wang and D. A. Sheen, *Prog. Energy Combust. Sci.*, 2015, **47**, 1–31.
36 N. Galagali and Y. M. Marzouk, *Chem. Eng. Sci.*, 2015, **123**, 170–190.
37 C. F. Goldsmith, A. S. Tomlin and S. J. Klippenstein, *Proc. Combust. Inst.*, 2013, **34**, 177–185.
38 L. Xing, S. Li, Z. Wang, B. Yang, S. J. Klippenstein and F. Zhang, *Combust. Flame*, 2015, **162**, 3427–3436.
39 L. Lei and M. P. Burke, *Combust. Flame*, 2020, **213**, 467–474.
40 T. Nagy and T. Turanyi, *Int. J. Chem. Kinet.*, 2011, **43**, 359–378.
41 C. M. Bishop, *Pattern Recognition and Machine Learning*, 2006, pp. 1–711.
42 A. Varnek, D. Fourches, F. Hoonakker and V. P. Solov'ev, *J. Comput.-Aided Mol. Des.*, 2005, **19**, 693–703.
43 W. H. Green, *Adv. Chem. Eng.*, 2007, **32**, 1–50.
44 P. Blowers and R. Masel, *AIChE J.*, 2000, **46**, 2041–2052.
45 C. W. Gao, M. Liu and W. H. Green, *Int. J. Chem. Kinet.*, 2020, **52**, 266–282.
46 A. Fridlyand, M. S. Johnson, S. S. Goldsborough, R. H. West, M. J. McNenly, M. Mehl and W. J. Pitz, *Combust. Flame*, 2017, **180**, 239–249.
47 K. P. Somers and J. M. Simmie, *J. Phys. Chem. A*, 2015, **119**, 8922–8933.
48 T. Nagy, E. Valko, I. Sedyo, I. G. Zsely, M. J. Pilling and T. Turanyi, *Combust. Flame*, 2015, **162**, 2059–2076.